Photochemical Production and Release of Gaseous NO_2 from Nitrate-Doped Water Ice

C. S. Boxe,[†] A. J. Colussi,*[,†] M. R. Hoffmann,[†] J. G. Murphy,[‡] P. J. Wooldridge,[‡] T. H. Bertram,[‡] and R. C. Cohen[‡]

W. M. Keck Laboratories, California Institute of Technology, Pasadena, California 91125, and Department of Chemistry and Department of Earth and Planetary Sciences, University of California, Berkeley, California 94720

Received: April 11, 2005; In Final Form: July 7, 2005

Temperature-programmed NO_2 emissions from frozen aqueous $NaNO_3$ solutions irradiated at 313 nm were monitored as function of nitrate concentration and heating rate, H, above −30 °C. Emissions increase nonmonotonically with temperature, displaying transitions suggestive of underlying metamorphic transformations. Thus, NO_2 emissions surge at ca. −8 °C in frozen $[NO_3^-] > 200$ μM samples warmed at $H = 0.70$ °C min^{-1} under continuous irradiation, and also in the dark from samples that had been photolyzed at −30 °C. The amounts of NO_2 released in individual thermograms, Σ_N, increase less than linearly with $[NO_3^-]$ or the duration of experiments, revealing the significant loss of photogenerated NO_2. The actual $\Sigma_N \propto [NO_3^-]^{1/2}$ dependence (at constant H) is consistent with NO_2 hydrolysis: $2NO_2 + H_2O \rightarrow NO_3^- + NO_2^- + 2H^+$, overtaking NO_2 desorption, even below the eutectic point (−18 °C for aqueous $NaNO_3$). The increasingly larger NO_2 losses detected in longer experiments (at constant $[NO_3^-]$) are ascribed to secondary photolysis of trapped NO_2. The relevance of present results to the interpretation of polar NO_2 measurements is briefly analyzed.

Introduction

The even distribution of nitrate across Greenland and Antarctica arises from remote sources convolved with long distance atmospheric transport.[1−4] Nitrate depth profiles in polar ice should provide, therefore, a valuable record of global paleoatmospheres, were they preserved over geological times. However, nitrate (molar absorptivity: $\epsilon_{310\ nm} = 7.5\ M^{-1}\ cm^{-1}$)[5,6] undergoes solar photolysis in the snowpack, thereby releasing NO_X into the overlying atmosphere,[7−16] and compromising its documental value.[6,17] The •OH radicals generated in reaction 1 and 3,[18−23] can also drive the oxidation of organic matter within snowpacks.[24−26]

$$NO_3^- + H^+ \xrightarrow{h\nu} NO_2 + {}^\bullet OH \quad (1)$$

$$NO_3^- \xrightarrow{h\nu} NO_2^- + O(^3P) \quad (2)$$

$$NO_2^- + H^+ \xrightarrow{h\nu} NO + {}^\bullet OH \quad (3)$$

The reaction medium in which these processes take place is deemed to remain fluid well below 0 °C because: (1) NO_2^- and NO_2 formation rates in ice and water do not exhibit discontinuities about the freezing point,[27−29] and (2) NO_2^- production rates are significantly enhanced by formate, as a nongeminate •OH scavenger, in both fluid and frozen solutions.[28] NO_X emission rates from irradiated frozen nitrate solutions are partially controlled by reaction 1:[27] photogenerated NO_2 is significantly delayed in subsurfacial layers prior to desorption.[27] We now report temperature-programmed NO_2 photodesorption rates from nitrate-doped polycrystalline ice as a function of nitrate concentration and heating rates that provide direct information on the mechanism and extent of nongeminate NO_2 reconversion into nitrate, and on the photolysis of trapped NO_2.

Experimental Methods

A schematic representation of the LIF detection setup, which is directly coupled to the photoreactor,[30] is shown in Figure 1. About 4−5 mL of pre-cooled aqueous $NaNO_3$ (EM Science) solutions (2 μM to 50 mM) was sprayed onto a coldfinger (CF in Figure 2, $A = 304$ cm^2) to produce nitrate-doped polycrystalline ice (NDI) layers with an average thickness of $\delta \sim 150$ μm. The ice temperature was controlled with an external cryogenic unit (Thermo Neslab ULT-80), which circulated refrigerated fluid through the interior of the CF. The ice-covered CF was encased within a sealed quartz sheath (QS), placed in a reflective cylindrical stainless steel chamber, and illuminated by four Hg Pen-Ray UV lamps (UVP, model 90-0001-04) emitting at $\lambda = 313 \pm 20$ nm. The photon irradiance incident on the QS, $I_i = 3.0 \times 10^{15}$ photons cm^2 s^{-1}, was determined using potassium ferrioxalate as a chemical actinometer.[31] The lamp stability was monitored by a photocell located on the top of the reflective chamber. The NDI matrixes, initially held at ca. −30 °C, were heated at $H = 0.70$, 0.30, or 0.10 °C min^{-1} up to 5 °C during or, in some specific experiments described below, after irradiation. The photogenerated NO_2 was continuously flushed with zero-air carrier gas, $F_C = 2.5$ L min^{-1} at 1 atm, into the detection zone.[30] Laser induced NO_2 fluorescence signals were detected with a sensitivity of 5 pptv/min.[30]

Results and Discussion

Under constant carrier gas flow rates, $NO_2(g)$, N_G, concentrations are directly proportional to net desorption rates, $R = k_d$-

* Address correspondence to this author. E-mail: ajcoluss@caltech.edu.
[†] California Institute of Technology.
[‡] University of California.

10.1021/jp0518815 CCC: $30.25
Published on Web 09/02/2005

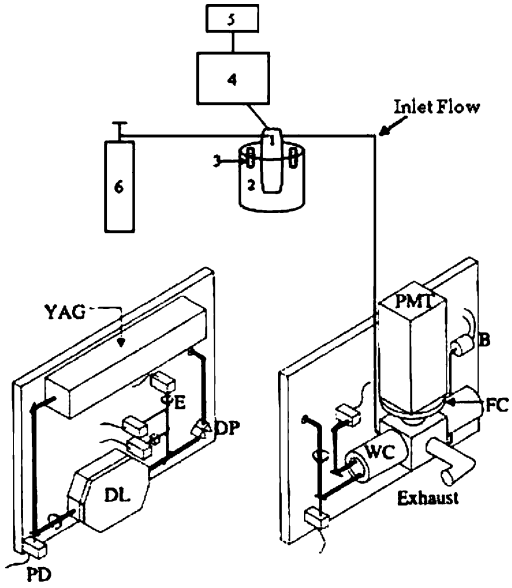

Figure 1. Schematic diagram of the experimental setup: (1) photolysis cell (see Figure 2); (2) reflective reaction chamber; (3) pen-ray UV lamps emitting at $\lambda_{max} \sim 313$ nm; (4) circulating cryostat; (5) computer workstation; and (6) zero air carrier gas. The Berkeley laser-induced fluorescence NO_2 instrument.[30] A frequency doubled YAG laser (YAG) pumps a dye laser (DL), whose output (585 nm) is sampled by fused silica beam splitters to monitor power, frequency, and line width (via Etalon E). Photodiode detectors (PD) monitor beam power. A dispersion prism (DP) selects 585 nm light from the beam, and directs it to a multipass White detection cell (WC), whose pressure is monitored with a 100 Torr Baratron capacitance manometer (B). NO_2 fluorescence is detected by a cooled PMT after being filtered through FC.

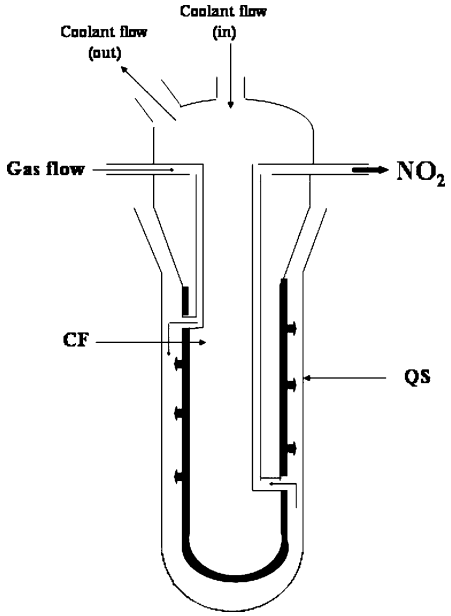

Figure 2. The photolytic reactor (1) of Figure 1. CF is the coldfinger on which polycrystalline ice is formed by spray freezing aqueous nitrate solutions. QS is a quartz sheath.

$[N_T]$, i.e., to the difference between primary photochemical production rates, J, minus the rates of accumulation, $\partial[N_T]/\partial t$, and chemical, C, or photochemical, D, destruction, of trapped NO_2, N_T:

$$R = k_d[N_T] = J - \partial[N_T]/\partial t - C - D = [N_G]F_C \quad (4)$$

Considering that the LIF detection zone is at 293 K, and $F_C = 41.7$ cm^3 s^{-1}, the detection of 1 pptv N_G (1 part in 10^{12} per volume $= 2.5 \times 10^7$ molecule cm^{-3} at 1 atm, 293 K) in this experimental setup is equivalent to the net release of $R = 1.0 \times 10^9$ N_G molecules s^{-1}, or 3.4×10^6 N_G molecules cm^{-2} s^{-1}, from the illuminated area.

Since the incident photon flux is $I_i = 3.0 \times 10^{15}$ photons cm^2 s^{-1}, and the primary quantum yield of NO_2 production in ice is $\phi_1 \sim 2 \times 10^{-3}$ over this temperature range,[17,29] the detection of $\sim$10 ppbv N_G at peak production from 50 mM $NaNO_3$ frozen layers (Figure 3a) would imply that about 0.6% of the incident light is absorbed by nitrate: $(10^4$ pptv$) \times (3.4 \times 10^6$ N_G molecules cm^{-2} s^{-1}$)/(3.0 \times 10^{15}$ photons cm^2 s^{-1}$)/(2 \times 10^{-3}) = 5.7 \times 10^{-3}$, at steady state, if $C = D = 0$. The fact that this fraction is 10 times larger than the actual absorbance of our $\sim$150 μm thick frozen 50 mM nitrate layers—(7.5 M^{-1} cm^{-1}) $\times$ (5×10^{-3} M) $\times$ (0.015 cm) $= 5.6 \times 10^{-4}$—proves that peak N_G release rates in these thermograms do not represent instantaneous photochemical production rates, but reflect nonstationary conditions in which N_T accumulated during the course of the experiment is largely desorbed in the final stages. Therefore, the effective rate and quantum yield of N_G release are expected to be, in general, significantly smaller than the rate and quantum yield ϕ_1 of N_T production via reaction 1,[17,29] depending on the morphology of the layer. The latter will determine the rate constant of N_T desorption, k_d, and, hence, the extent of secondary NO_2 losses.

Accordingly, the $[N_G]$ vs T dependences shown in Figure 3a−f are not expected to be exclusively, or largely, determined by the temperature dependence of J, which primarily arises from the monotonic, exponential temperature dependence of ϕ_1,[17,29] but also from the existence of metamorphic transitions via $k_d(T)$, and, as appropriate to transient phenomena, from H and $[NO_3^-]$ as well. It is apparent that the upward inflection observed in $[NO_2]$ at ca. −8 °C for $[NO_3^-] = 50$ mM, $H = 0.7$ °C min^{-1} (Figure 3a) gradually disappears at lower $[NO_3^-]$. Emission rates sharply decrease above ca. −4 °C, following the depletion of accumulated N_T due to an artifact: thawed solutions fall to the QS bottom where they receive less radiation than as NDI's.

Previously, we rationalized similar observations by assuming that photogenerated N_T lines the microscopic cavities of polycrystalline ice before desorbing into the gas phase. The fraction of N_G filling the network of cavities connected to the atmosphere diffuses/effuses away concomitantly with photolysis, while the rest remains occluded in closed pockets until they open up during the softening of the ice matrix at higher temperatures. The existence of N_T and the heterogeneous mechanism underlying the sharp transitions observed in the thermograms is confirmed by decoupling photolysis and desorption: in the experiments shown in Figure 4a,b $[NO_3^-] = 50$ mM NDI's were illuminated for 3 h at −30 °C, and then heated at $H = 0.70$ °C min^{-1} in the dark. The protracted approach to a steady-state value of $\sim$6.5 ppbv N_G under isothermal conditions, vs the relatively fast responses observed in the thermograms at low temperatures (see Figure 7b below), suggests that the system is reaching equilibrium via a slow chemical reaction. N_G emissions rapidly fall off after photolysis and display a distinctive surge at ca. −8 °C in the dark, analogous to that observed in the bright thermogram of Figure 3a. A similar isothermal experiment at $[NO_3^-] = 2$ μM, −30 °C is shown in Figure 5a,b. In this case, average $\sim$240 pptv N_G emissions during 3.2 h amount to the release of $\sim 3 \times 10^{15}$ NO_2 molecules, or to the photolysis of $\sim$50% of the nitrate contained in $\sim$5 cm^3 of 2 μM $NaNO_3$. In contrast to the results of Figure 4a, the slow decline of N_G emissions during the experiment shown in Figure 5a reflects the gradual depletion

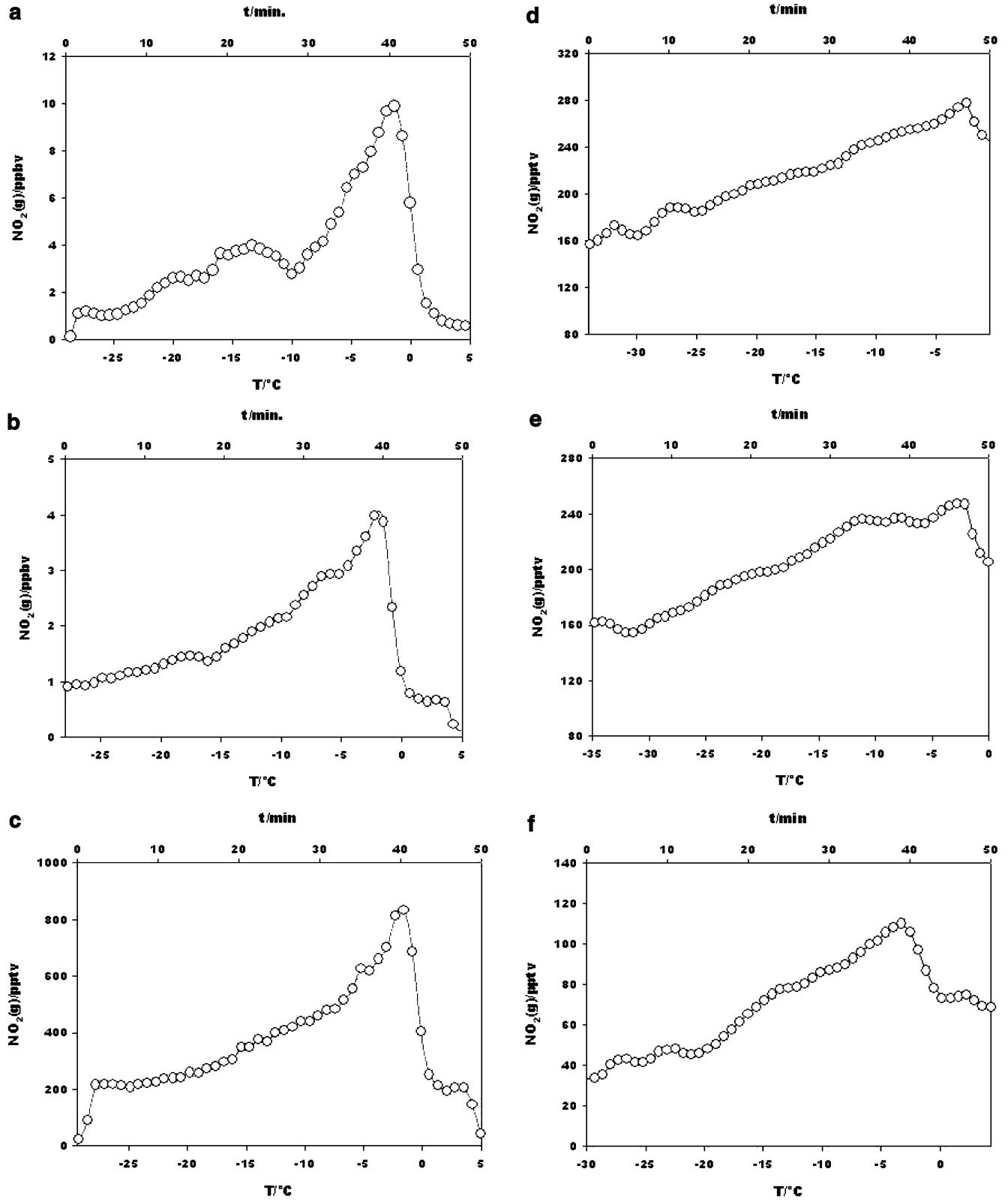

Figure 3. (a) NO_2(g) concentration vs temperature during irradiation of frozen 50 mM aqueous nitrate under $H = 0.70$ °C min^{-1}. (b) NO_2(g) concentration vs temperature during irradiation of frozen 10 mM aqueous nitrate under $H = 0.70$ °C min^{-1}. (c) NO_2(g) concentration vs temperature during irradiation of frozen 1 mM aqueous nitrate under $H = 0.70$ °C min^{-1}. (d) NO_2(g) concentration vs temperature during irradiation of frozen 0.2 mM aqueous nitrate under $H = 0.70$ °C min^{-1}. (e) NO_2(g) concentration vs temperature during irradiation of frozen 30 μM aqueous nitrate under $H = 0.70$ °C min^{-1}. (f) NO_2(g) concentration vs temperature during irradiation of frozen 2 μM aqueous nitrate under $H = 0.70$ °C min^{-1}.

of nitrate. Notice that if N_G emissions were directly proportional to $[NO_3^-]$, as expected for a system in which all processes were first order in (N_T, N_G), the limiting N_G value for $[NO_3^-] = 50$ mM should be 0.24 ppbv × (50 mM/2μM) = 6 ppmv, rather than 6.5 ppbv as observed.

Evidence that nitrate photolysis and N_T desorption are not the only relevant processes in this system is provided by the fact that the total amount of NO_2, $\Sigma_N = \int[N_G]F_C\, dt$, released over the course of a photochemical experiment is proportional to $[NO_3^-]^{1/2}$ at $H = 0.70$ °C min^{-1} (Figure 6). Since desorption

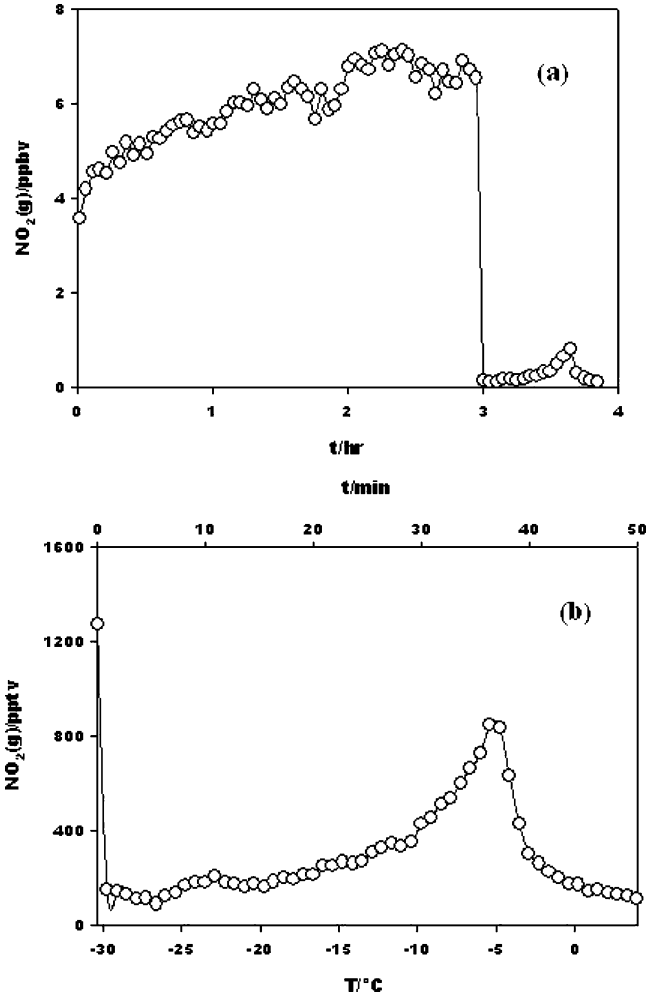

Figure 4. (a) NO_2(g) concentrations above frozen 50 mM aqueous nitrate irradiated at −30 °C for 3 h and then warmed at $H = 0.70$ °C min^{-1} in the dark. (b) A blowup of part a after 3 h.

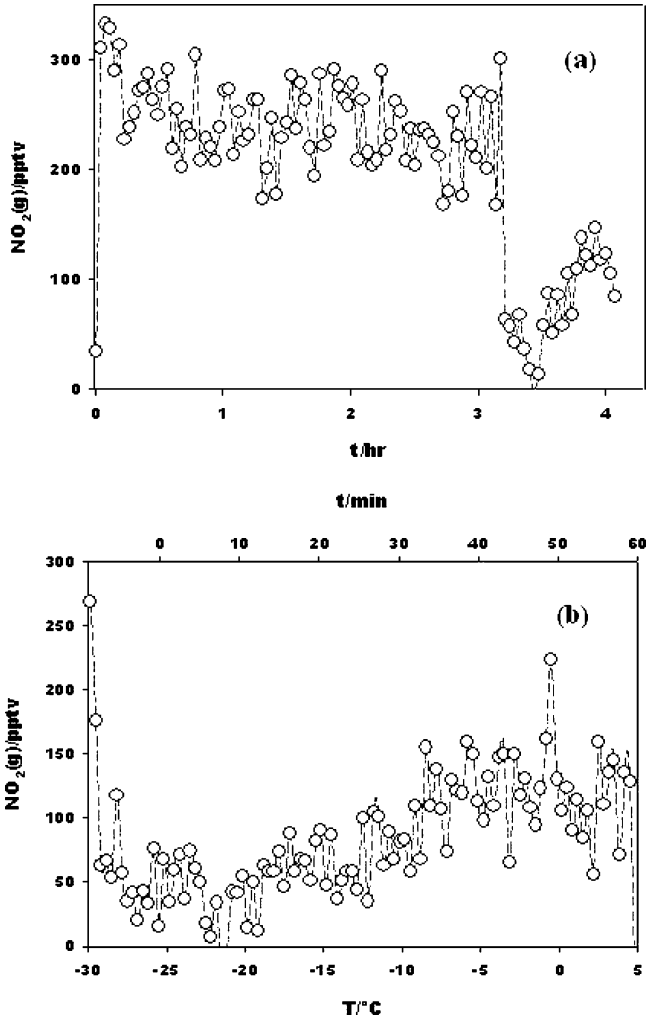

Figure 5. (a) NO_2(g) concentrations above frozen 2 μM aqueous nitrate irradiated at −30 °C for 3.25 h, and then warmed at $H = 0.70$ °C min^{-1} in the dark. (b) A blowup of part a after 3.25 h.

could only delay N_G emissions, and all NDI samples are optically thin, i.e., absorb less that 1% of the incident photon flux (see above), photolysis rates, J, and, hence, Σ_N should increase linearly with $[NO_3^-]$, *in the absence of loss processes with higher than first-order NO_2 dependences*, at variance with the results of Figure 6. Clearly, the $\Sigma_N \propto [NO_3^-]^{1/2}$ dependence cannot originate, solely, in the secondary photolysis of NO_2, another complicating feature considered below in more detail.

The second-order hydrolytic disproportionation of NO_2, reaction 5

$$2NO_2(g) + H_2O(l) \rightleftarrows NO_3^-(aq) + NO_2^-(aq) + 2H^+(aq) \quad (5)$$

has the required stoichiometry to produce the observed $\Sigma_N \propto [NO_3^-]^{1/2}$ dependence. Equilibrium constants, $K_5(T)$, can be calculated from $\Delta H_5 = -106.7$ kJ mol^{-1} and $\Delta S_5 = -278.7$ J K^{-1} mol^{-1}.[32] Let us estimate the equilibrium N_G pressure, P_{NO_2}, in reaction 5 at the eutectic, the minimum temperature at which H_2O(l) is present as a macroscopic phase. At the eutectic point, $T = 255$ K, and $K_5 = 2.2 \times 10^7$ (in M, atm units), 5.9 M $NaNO_3$ (45.5 M H_2O) is in equilibrium with pure ice and $NaNO_3$(s).[33] An upper limit to NO_2^-(aq) concentrations can be obtained from the difference between the expected and observed N_G emissions in Figure 5a (see above), and the stoichiometry of reaction 5: $[NO_2^-] < 0.2\ [NO_3^-] \sim 1$ M. Therefore, P_{NO_2}(atm) $< 8 \times 10^{-5}\ [H^+]$. Assuming pH >5.0, we find that P_{NO_2} could not exceed 0.8 ppbv at 255 K. The $P_{NO_2} \sim 0.2$ ppbv detected at −18 °C in the dark thermogram of Figure 5b is, therefore, compatible with the expected value.

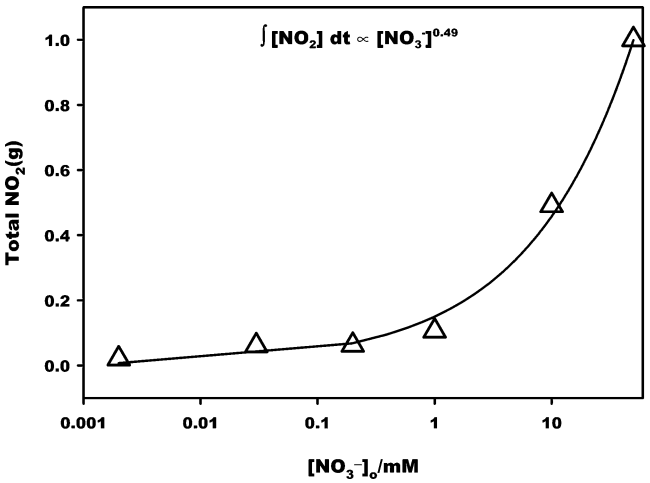

Figure 6. Total NO_2(g) amounts released during the photolysis of frozen aqueous nitrate solutions warmed at $H = 0.70$ °C min^{-1} vs $[NO_3^-]$. Total amounts are normalized to those measured in frozen 50 mM nitrate.

The rates of reaction 5 at the low NO_2 concentrations prevalent in the present experiments are expected to be second order in $[NO_2]$.[34] Thus, at steady state, eq 4 predicts that $k_5 P_{NO_2}^2$

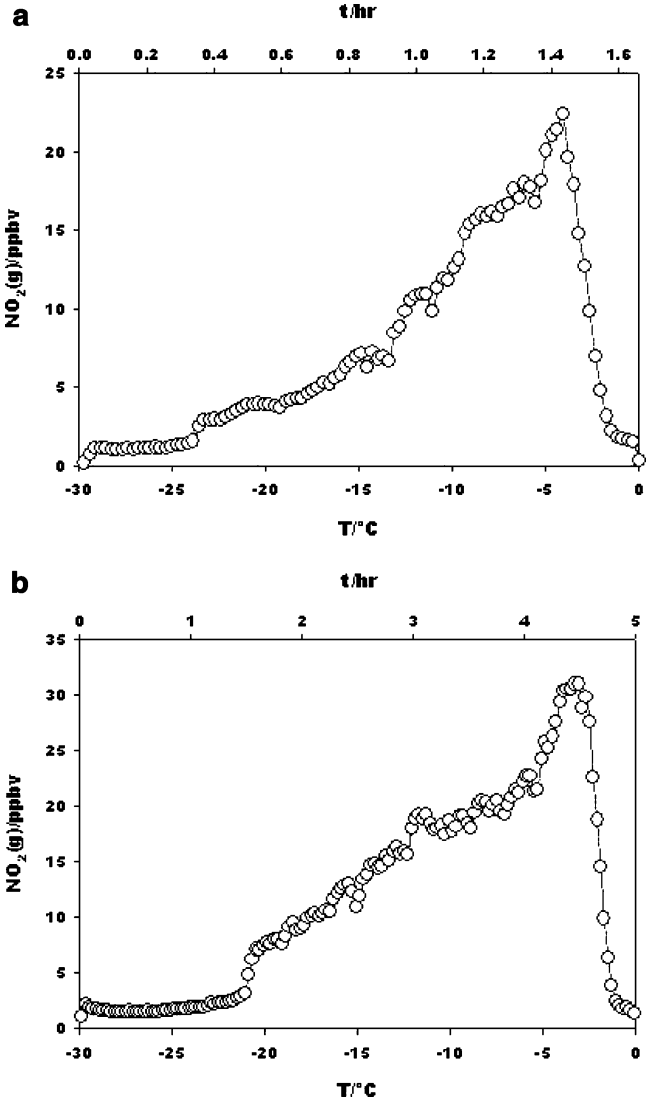

Figure 7. (a) NO_2(g) concentration vs temperature during irradiation of frozen 50 mM aqueous nitrate under $H = 0.30$ °C min^{-1}. (b) NO_2-(g) concentration vs temperature during irradiation of frozen 50 mM aqueous nitrate under $H = 0.10$ °C min^{-1}.

$\sim J \propto [NO_3^-]$, or $P_{NO_2} \propto [NO_3^-]^{1/2}$, if $D = 0$, and NO_2 hydrolysis were faster than desorption. This limit is eventually approached at sufficiently large $[NO_3^-]$ values, since desorption rates, $k_d[N_T] = k_d H^{-1} P_{NO_2}$ (H is Henry's constant for NO_2 in water) increase linearly with P_{NO_2}. The new finding is that extensive, relatively fast NO_2 hydrolysis, reaction 4, occurs on ice at least 12 °C below the eutectic point (cf. Figures 4a and 5a).

Since the time required to sweep the entire temperature range (from − 30 °C to above melting) is inversely proportional to the heating ramp, H, Σ_N should be, barring secondary losses, directly proportional to H^{-1} in experiments performed at constant $[NO_3^-]$. Panels a and b of Figure 7 show thermograms performed on $[NO_3^-] = 50$ mM NDI at $H = 0.30$ and 0.10 °C min^{-1}, respectively. These results, in conjunction with those of Figure 3a for $H = 0.70$ °C min^{-1}, as well as those performed on $[NO_3^-] = 2$ μM NDI (not shown), are presented in Figure 8. It is apparent that Σ_N vs H^{-1} plots are not linear: Σ_N only increases about 3-fold upon a 7-fold extension of photolysis time. The larger NO_2 deficits incurred under the slower heating ramps imply that N_T desorption becomes more favorable than chemical and/or photochemical loss reactions at higher temperatures. Thus, NO_2 production is not only a function of T and $[NO_3^-]$, but also of the thermal history of the irradiated sample in these time scales. The molar absorptivity of NO_2(g), averaged over the output of our lamps, is ∼28 times larger than that of NO_3^-.[29] If trapped NO_2 spent a small fraction of the time as N_G rather than as N_T, the larger quantum yield of NO_2-(g) photolysis

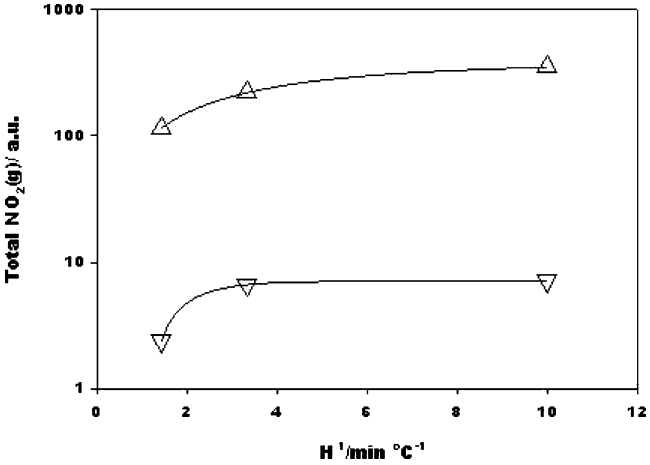

Figure 8. Total NO_2(g) amounts released during the photolysis of frozen aqueous nitrate solutions as function of the reciprocal of the heating rate H: (∇) $[NO_3^-] = 2$ μM and (Δ) $[NO_3^-] = 50$ mM.

$$NO_2 \xrightarrow{h\nu} NO + O(^3P) \qquad (6)$$

$\phi_6 \sim 1$ vs $\phi_1 \sim 8\phi_2 \sim 2 \times 10^{-3}$, would make reaction 6 dominate the NO_2 photodecomposition lifetime. Slow chemical losses due to secondary radical reactions may also contribute to the nonlinearity of the plots of Figure 8.[28,29]

Implications for Snowpack Chemistry in Polar Regions

The NO_3^- concentrations measured in snow at rural and remote sites range from 1 to 20 μM.[5,51−54] These overlap with the lower $[NO_3^-]$ range of the present experiments. Considering that nitrate samples were subjected to photon irradiances and temperatures of environmental relevance, our results can be used to interpret NO_2 emissions from sunlit snowpacks. Chu and Anastasio have recently compared the results of laboratory studies on the photochemistry of frozen nitrate solutions with field measurements of NO_x gases released during spring at various high-latitude locations.[17] Their analysis involves equating NO_2 release rates with the •OH production rates measured using benzoic acid as a •OH scavenger, as expected from the stoichiometry of reaction 1. Present experiments demonstrate that this cannot be the case because NO_2 desorption from polycrystalline ice is not instantaneous. While trapped in the ice, NO_2 is irreversibly transformed into other species through various pathways. Therefore, the apparent agreement between field NO_2 emissions and the estimates made in ref 17 on the basis of •OH production rates in the photolysis of NDI is probably fortuitous. We suggest, however, that agreement still would be possible if the species resulting from the decay of NO_2 in ice, such as NO and NO_2^-/HONO, were eventually released into the boundary layer, and therefore accounted for as NO_X. The $\Sigma_N \propto [NO_3^-]^{1/2}$ dependence provides a possible rationalization, at least in part, for the fact that noontime NO_X fluxes emitted from snowpacks, R_{NO_X}, only increase from $R_{NO_X} \sim 2.5 \times 10^8$ molecule cm^{-2} s^{-1} at $30 \leq [NO_3^-]$/ng $g_{ice}^{-1} \leq 100$ over Neumayer Station, Antarctica,[57] to $R_{NO_X} \sim 5 \times 10^8$ molecule cm^{-2} s^{-1} at $350 \leq [NO_3^-]$/ng $g_{ice}^{-1} \leq 560$ at the Alert station, Canada.[8]

Conclusions

The dependence of NO_2 emission rates on nitrate concentration and heating rates in the temperature-programmed photolysis of nitrate-doped polycrystalline ice demonstrates that photogenerated NO_2 undergoes extensive chemical and photochemical losses prior to desorption under typical conditions. The hydrolytic disproportionation of photogenerated NO_2 into nitrate and nitrite is the dominant dark loss pathway in ice, even at subeutectic temperatures.

Acknowledgment. C.S.B. acknowledges support from the Betty and Gordon Moore Foundation. This work was financed by NSF grant ATM-0228140.

References and Notes

(1) Platt, U. *The Origin of Nitrous and Nitric Acid in the Atmosphere*; Springer-Verlag: New York, 1986; Vol. G6.
(2) Logan, J. A. *J. Geophys. Res.* **1983**, *88*, 10785.
(3) Legrand, M.; Mayewski, P. *Rev. Geophys.* **1997**, *35*, 219.
(4) Mulvaney, R.; Wagenbach, D.; Wolff, E. W. *J. Geophys. Res.* **1998**, *103*, 11021.
(5) Dibb, J. E.; Talbot, R. W.; Munger, J. W.; Jacob, D. J.; Fan, S. M. *J. Geophys. Res.* **1998**, *103*, 3475.
(6) Wolff, E. W. *Nitrate in Polar Ice*; Springer-Verlag: New York, 1995; Vol. I30.
(7) Beine, H. J.; Domine, F.; Ianniello, A.; Nardino, M.; Allegrini, I.; Teinila, K.; Hillamo, R. *Atmos. Chem. Phys.* **2003**, *3*, 335.
(8) Beine, H. J.; Domine, F.; Simpson, W.; Honrath, R. E.; Sparapani, R.; Zhou, X. L.; King, M. *Atmos. Environ.* **2002**, *36*, 2707.
(9) Beine, H. J.; Honrath, R. E.; Domine, F.; Simpson, W. R.; Fuentes, J. D. *J. Geophys. Res.* **2002**, *107*.
(10) Dibb, J. E.; Arsenault, M.; Peterson, M. C.; Honrath, R. E. *Atmos. Environ.* **2002**, *36*, 2501.
(11) Honrath, R. E.; Lu, Y.; Peterson, M. C.; Dibb, J. E.; Arsenault, M. A.; Cullen, N. J.; Steffen, K. *Atmos. Environ.* **2002**, *36*, 2629.
(12) Davis, D.; Nowak, J. B.; Chen, G.; Buhr, M.; Arimoto, R.; Hogan, A.; Eisele, F.; Mauldin, L.; Tanner, D.; Shetter, R.; Lefer, B.; McMurry, P. *Geophys. Res. Lett.* **2001**, *28*, 3625.
(13) Peterson, M. C.; Honrath, R. E. *Geophys. Res. Lett.* **2001**, *28*, 511.
(14) Ridley, B.; Walega, J.; Montzka, D.; Grahek, F.; Atlas, E.; Flocke, F.; Stroud, V.; Deary, J.; Gallant, A.; Boudries, H.; Bottenheim, J.; Anlauf, K.; Worthy, D.; Sumner, A. L.; Splawn, B.; Shepson, P. *J. Atmos. Chem.* **2000**, *36*, 1.
(15) Jones, A. E.; Weller, R.; Wolff, E. W.; Jacobi, H. W. *Geophys. Res. Lett.* **2000**, *27*, 345.
(16) Honrath, R. E.; Peterson, M. C.; Guo, S.; Dibb, J. E.; Shepson, P. B.; Campbell, B. *Geophys. Res. Lett.* **1999**, *26*, 695.
(17) Chu, L.; Anastasio, C. *J. Phys. Chem. A* **2003**, *107*, 9594.
(18) Mack, J.; Bolton, J. R. *J. Photochem. Photobiol., A* **1999**, *128*, 1.
(19) Mark, G.; Korth, H. G.; Schuchmann, H. P.; vonSonntag, C. *J. Photochem. Photobiol., A* **1996**, *101*, 89.
(20) Alif, A.; Boule, P. *J. Photochem. Photobiol., A* **1991**, *59*, 357.
(21) Zellner, R.; Exner, M.; Herrmann, H. *J. Atmos. Chem.* **1990**, *10*, 411.
(22) Warneck, P.; Wurzinger, C. *J. Phys. Chem.* **1988**, *92*, 6278.
(23) Zepp, R. G.; Hoigne, J.; Bader, H. *Environ. Sci. Technol.* **1987**, *21*, 443.
(24) Sumner, A. L.; Shepson, P. B. *Nature* **1999**, *398*, 230.
(25) Domine, F.; Shepson, P. B. *Science* **2002**, *297*, 1506.
(26) Bilski, P.; Chignell, C. F.; Szychlinski, J.; Borkowski, A.; Oleksy, E.; Reszka, K. *J. Am. Chem. Soc.* **1992**, *114*, 549.
(27) Boxe, C. S.; Colussi, A. J.; Hoffmann, M. R.; Tan, D.; Mastromarino, J.; Case, A. T.; Sandholm, S. T.; Davis, D. D. *J. Phys. Chem. A* **2003**, *107*, 11409.
(28) Dubowski, Y.; Colussi, A. J.; Boxe, C.; Hoffmann, M. R. *J. Phys. Chem. A* **2002**, *106*, 6967.
(29) Dubowski, Y.; Colussi, A. J.; Hoffmann, M. R. *J. Phys. Chem. A* **2001**, *105*, 4928.
(30) Thornton, J. A.; Wooldridge, P. J.; Cohen, R. C. *Anal. Chem.* **2000**, *72*, 528.
(31) Calvert, J.; Pitts, J. N. *Photochemistry*; Wiley: New York, 1966.
(32) Schwartz, S. E.; White, W. H. *Adv. Environ. Sci. Eng.* **1981**, *4*, 1.
(33) Seidell, A. *Solubilities of Inorganic and Metal Organic Compounds*, 3rd ed.; van Nostrand: New York, 1940; Vol. 1.
(34) Schwartz, S. E.; White, W. H. *Adv. Environ. Sci. Technol.* **1983**, *12*, 1.
(35) Rempel, A. W.; Waddington, E. D.; Wettlaufer, J. S.; Worster, M. G. *Nature* **2001**, *411*, 568.
(36) Killawee, J. A.; Fairchild, I. J.; Tison, J. L.; Janssens, L.; Lorrain, R. *Geochim. Cosmochim. Acta* **1998**, *62*, 3637.
(37) Takenaka, N.; Ueda, A.; Daimon, T.; Bandow, H.; Dohmaru, T.; Maeda, Y. *J. Phys. Chem.* **1996**, *100*, 13874.
(38) Dash, J. G.; Fu, H. Y.; Wettlaufer, J. S. *Rep. Prog. Phys.* **1995**, *58*, 115.
(39) Gross, G. W.; Gutjahr, A.; Caylor, K. *J. Phys.* **1987**, *48*, 527.
(40) Gross, G. W.; Wong, P. M.; Humes, K. *J. Chem. Phys.* **1977**, *67*, 5264.
(41) Gross, G. W.; McKee, C.; Wu, C. H. *J. Chem. Phys.* **1975**, *62*, 3080.
(42) Gross, G. W. *Adv. Chem. Ser.* **1968**, 27.
(43) Ewing, G. E. *J. Phys. Chem. B* **2004**, *108*, 15953.
(44) Menzel, M. I.; Han, S. I.; Stapf, S.; Blumich, B. *J. Magn. Reson.* **2000**, *143*, 376.
(45) Cho, H.; Shepson, P. B.; Barrie, L. A.; Cowin, J. P.; Zaveri, R. *J. Phys. Chem. B* **2002**, *106*, 11226.
(46) Henson, B. F.; Robinson, J. M. *Phys. Rev. Lett.* **2004**, *92*, 246107.
(47) Hindmarsh, J. P.; Buckley, C.; Russell, A. B.; Chen, X. D.; Gladden, L. F.; Wilson, D. I.; Johns, M. L. *Chem. Eng. Sci.* **2004**, *59*, 2113.
(48) Fukazawa, H.; Sugiyama, K.; Mae, S. J.; Narita, H.; Hondoh, T. *Geophys. Res. Lett.* **1998**, *25*, 2845.
(49) Nye, J. F. *J. Glaciol.* **1989**, *35*, 17.
(50) Mulvaney, R.; Wolff, E. W.; Oates, K. *Nature* **1988**, *331*, 247.
(51) De Angelis, D.; Legrand, M. Ice Core Studies of Global Biogeochemical Cycles. *NATO ASI Ser., Ser. 1* **1995**, *30*, 361.
(52) Silvente, E.; Legrand, M. Ice Core Studies of Global Biogeochemical Cycles. *NATO ASI Ser., Ser. 1* **1995**, *30*, 225.
(53) Jaffe, D. A.; Zukowski, M. D. *Atmos. Environ.* **1993**, *27*, 2935.
(54) Stottlemyer, R.; Toczydlowski, D. *Can. J. Fish. Aquat. Sci.* **1990**, *47*, 290.